nature physics

Article

https://doi.org/10.1038/s41567-024-02493-1

Single-component superconductivity in UTe₂ at ambient pressure

Received: 19 July 2023

Accepted: 28 March 2024

Published online: 9 May 2024

Check for updates

Florian Theuss \mathbb{O}^1 , Avi Shragai¹, Gaël Grissonnanche $\mathbb{O}^{1,2,3}$, Ian M. Hayes \mathbb{O}^4 , Shanta R. Saha⁴, Yun Suk Eo \mathbb{O}^4 , Alonso Suarez⁴, Tatsuya Shishidou \mathbb{O}^5 , Nicholas P. Butch $\mathbb{O}^{4,6}$, Johnpierre Paglione $\mathbb{O}^{4,7}$ & B. J. Ramshaw $\mathbb{O}^{1,7}$

The microscopic mechanism of Cooper pairing in a superconductor leaves its fingerprint on the symmetry of the order parameter. UTe₂ has previously been inferred to have a multi-component order parameter, in part due to the apparent presence of a two-step superconducting transition in some samples. However, recent experimental observations in newer-generation samples have raised questions about this interpretation, pointing to the need for a direct probe of the order parameter symmetry. Here we use pulse-echo ultrasound to measure the elastic moduli of UTe₂ in samples that exhibit both one and two superconducting transitions. We demonstrate the absence of thermodynamic discontinuities in the shear elastic moduli of both single- and double-transition samples, providing direct evidence that UTe₂ has a single-component superconducting order parameter. We further show that superconductivity is highly sensitive to compression strain along the a and c axes but insensitive to strain along the b axis. This leads us to suggest a single-component, odd-parity order parameter—specifically the B_{2u} order parameter—as most compatible with our data.

Definitive determination of the superconducting pairing symmetry has been accomplished for only a handful of materials, among them the s-wave Bardeen–Cooper–Schrieffer superconductors and the d-wave cuprates¹. In some superconductors, such as Sr₂RuO₄, debate over the pairing symmetry has persisted for decades despite ultra-pure samples and an arsenal of experimental techniques²-⁴. This is more than an issue of taxonomy: the pairing symmetry places strong constraints on the microscopic mechanism of Cooper pairing, and some pairing symmetries can lead to topological superconducting states⁵.

The question of pairing symmetry is nowhere more relevant than in UTe₂, where in addition to power laws in thermodynamic quantities ^{6–9}, the most striking evidence for unconventional superconductivity is an extremely high upper critical field $H_{\rm c2}$ compared with the relatively low critical temperature ^{7,10}. Remarkably, for some field orientations, the superconductivity re-emerges from a resistive state above

approximately 40 T and persists up to at least 60 T (ref. 11). This high H_{c2} constrains the spin component of the Cooper pair to be spin-triplet, which in turn constrains the orbital component of the Cooper pair to be odd under inversion (that is odd parity, such as a p- or f-wave state). However, there are many possible odd-parity order parameters and which one—or which pair, if UTe $_2$ is a two-component superconductor as suggested 12 —manifests in UTe $_2$ is unknown.

The primary question we address here is regarding the degeneracy of the orbital part of the superconducting order parameter. In addition to even (s- or d-wave) and odd (p- and f-wave) designations, order parameters can have multiple components: both conventional s-wave and high- $T_c d_{\chi^2-y^2}$ -wave order parameters are described by a single complex number, whereas the topological p_x + ip_y state has two components, namely p_x and p_y . Evidence for a two-component order parameter in UTe₂ stems from the presence of two distinct superconducting

¹Laboratory of Atomic and Solid State Physics, Cornell University, Ithaca, NY, USA. ²Kavli Institute at Cornell for Nanoscale Science, Ithaca, NY, USA. ³Laboratoire des Solides Irradiés, CEA/DRF/IRAMIS, CNRS, École Polytechnique, Institut Polytechnique de Paris, Palaiseau, France. ⁴Maryland Quantum Materials Center, Department of Physics, University of Maryland, College Park, MD, USA. ⁵Department of Physics, University of Wisconsin-Milwaukee, Milwaukee, WI, USA. ⁶NIST Center for Neutron Research, National Institute of Standards and Technology, Gaithersburg, MD, USA. ⁷Canadian Institute for Advanced Research, Toronto, Ontario, Canada. ⊠e-mail: bradramshaw@cornell.edu

Table 1 | Proposed order parameters for UTe,

Dimensionality	Representation	Shear discontinuity?	Reference (E, experiment; T, theory)	
			E: NMR ³⁰	
One component	A_u	No	E: scanning SQUID ³¹	
	B_{2u}	No	E: ultrasound (this work)	
	B_{3u}		T: DFT ³²	
		No	E: NMR ^{33,34}	
			E: scanning SQUID ³¹	
		No	E: specific heat ^{16,17}	
		INO	E: uniaxial stress ²⁶	
	$\{B_{1\omega},A_{\omega}\}$	C ₆₆	E: microwave surface impedance ¹⁵	
			E: specific heat, Kerr effect ¹²	
	$\{B_{3u},A_u\}$	C ₄₄	E: penetration depth ⁸	
			E: NMR ³⁵	
	$\{B_{1u}, B_{2u}\}$	C ₄₄	T: ³ He A-phase-like pairing ^{36,37}	
			E: specific heat ⁹	
Two component	$\{B_{1u},B_{3u}\}$	C ₅₅	T: phenomenology + DFT ³⁸	
			T: DFT ³⁹	
	$\{B_{2u},B_{3u}\}$		T: DFT ^{22,23}	
		C ₆₆	E: specific heat, Kerr effect ^{12,13}	
			T: emergent D _{4h} symmetry ²⁴	
			E: STM ¹⁴	
		Yes	T: pair-Kondo effect ⁴⁰	
			T: MFT of Kondo lattice ⁴¹	

Proposed odd-parity order parameters for UTe_2 , sorted by the number of components (dimensionality), their irreducible representation and whether the proposed order parameter is based on an experimental observation or a theoretical proposal. Scenarios listed without a specific representation are compatible with any type of one- or two-component order parameter. On the basis of symmetry alone, our work strongly constrains the order parameter to be of the one-component type. Using more quantitative arguments, we suggest a B_{2u} order parameter. NMR, nuclear magnetic resonance; SQUID, superconducting quantum interference device; DFT, density functional theory.

transitions in some samples, as well as from the onset of time-reversal symmetry breaking at $T_{\rm c}$ (refs. 12,13). Combined with evidence for spin-triplet pairing, these observations have led to several proposed exotic, multi-component order parameters for UTe₂ (Table 1). These multi-component states can have a topological structure that could explain other experimental observations, such as the chiral surface states seen in scanning tunnelling microscopy (STM)¹⁴ or the anomalous normal component of the conductivity observed in microwave impedance measurements¹⁵.

Claims of a multi-component order parameter are not without controversy, however. As the purity of the samples has increased, $T_{\rm c}$ has shifted to higher values and the second transition has disappeared at ambient pressure 16. Previous work has suggested that two transitions arise due to inhomogeneity 17, but the application of hydrostatic

pressure splits single- T_c samples into two- T_c samples 18,19 , suggesting that two superconducting order parameters are, at the very least, nearly degenerate with one another.

The natural way to distinguish between single-component and two-component order parameters is to apply strain. Single-component superconductors have a single degree of freedom—the superfluid density—that couples to compression strains, producing a discontinuity in the compressional elastic moduli at $T_{\rm c}$ (Fig. 1). Single-component superconductors, however, have no such discontinuity in their shear moduli because shear strains preserve volume and thus do not couple to superfluid density. Multi-component superconductors, on the other hand, have additional degrees of freedom: the relative orientation of the two order parameters, as well as their relative phase difference. These additional degrees of freedom couple to shear strains, producing discontinuities in the shear moduli at $T_{\rm c}$. By identifying which elastic moduli have discontinuities at $T_{\rm c}$, one can determine whether a superconductor is multi-component without any microscopic knowledge of the Fermi surface or the pairing mechanism.

Results

We use a traditional phase-comparison pulse-echo ultrasound technique to measure the temperature dependence of six elastic moduli in three different samples of UTe₂ over a temperature range from approximately 1.3 to 1.9 K. In particular, we measure all three compressional (that is, c_{11} , c_{22} and c_{33}) and shear (that is, c_{44} , c_{55} and c_{66}) moduli in one sample with two superconducting transitions (S3: $T_{c,1} \approx 1.64$ K, $T_{c,2} \approx 1.60$ K) and in two samples with a single T_c (S1: $T_c \approx 1.63$ K and S2: $T_c \approx 1.70$ K). Ultrasound data in the normal state of UTe₂ have been reported by Ushida et al. 20 . Here, we focus on the superconducting transition. Details of the sample growth and preparation, as well as the experiment, are given in Methods.

Figure 2 shows the relative changes in four elastic moduli across $T_{\rm c}$ for the single-transition samples S1 and S2. We observe a single, sharp (approximately 85 mK wide) discontinuity in the c_{33} compressional modulus, as expected for all superconducting transitions. We observe no discontinuities in any of the shear elastic moduli to within our experimental resolution (a few parts in 10^7 ; see Supplementary Figs. 5 and 6 for details).

Figure 3 shows the relative changes in the elastic moduli for sample S3 with a double superconducting transition (the single- T_c data are reproduced here for comparison). We observe two distinct discontinuities in c_{33} separated by approximately 40 mK. Subsequent specific heat measurements on the same sample show a similar double peak feature identified in other double- T_c samples (specific heat data are shown in Supplementary Fig. 7). Notably, we find the sum of the discontinuities in the double- T_c sample to be of a similar size as the discontinuity in the single- T_c sample. Additionally, the behaviour of the shear elastic moduli is nearly identical to that of the single- T_c samples, again with no discontinuities at T_c .

We also measure the two other compressional moduli– $c_{\rm II}$ and $c_{\rm 22}$ —and show them along with $c_{\rm 33}$ in Fig. 4. $c_{\rm II}$ has a discontinuity of approximately 20 parts per million—roughly a factor of 2 smaller than the discontinuity in $c_{\rm 33}$. In contrast, $c_{\rm 22}$ has a discontinuity of at most 1 part per million—significantly smaller than the other two compressional moduli. Discontinuities in all three compressional moduli are allowed by symmetry for any superconducting order parameter (see ref. 2 and 'Landau free energy calculations' section in Supplementary Information).

We first analyse the data using only the presence or absence of discontinuities in the elastic moduli. This analysis is based on symmetry arguments alone and is independent of the size of the discontinuities. We then perform a quantitative analysis of the discontinuities using Ehrenfest relations. Finally, we combine all of our observations to speculate on which particular superconducting order parameter is most consistent with our data.

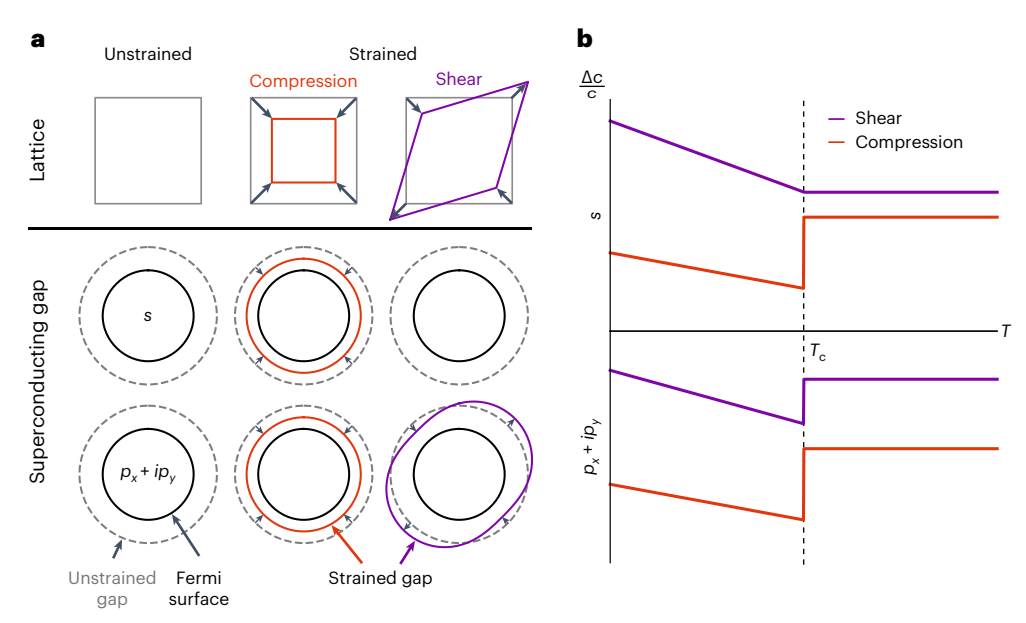


Fig. 1| **The influence of strain on one- and two-component superconductors. a**, An illustration of how two representative order parameters—single-component s-wave and two-component p_x + ip_y —respond to both compression and shear strain. Both gaps respond under compression (whether increasing or decreasing in magnitude depends on microscopic details). Only the two-

component gap, however, couples to shear strain—here we illustrate the phase mode (see ref. 2 for more details). **b**, The expected changes in elastic moduli across T_c for one- and two-component order parameters. All superconductors have a discontinuity in their compressional moduli across T_c , but only two-component superconductors have discontinuities in their shear moduli.

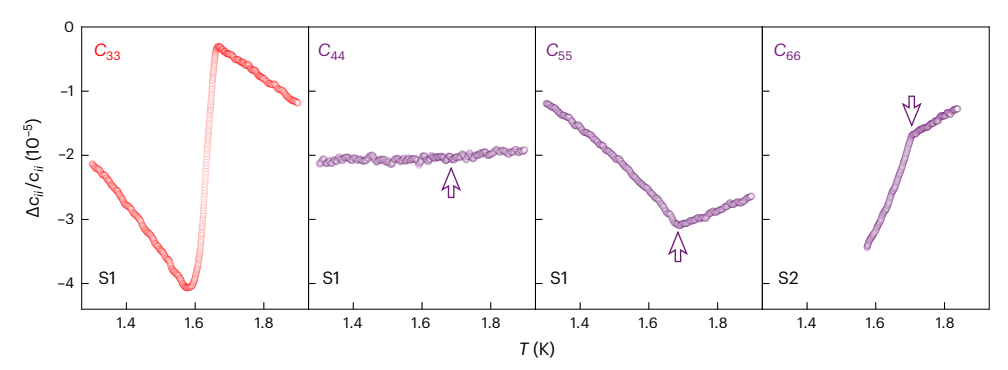


Fig. 2| **Relative change in elastic moduli through** T_c **for single-** T_c **UTe₂.** The compressional elastic modulus c_{33} shows a sharp discontinuity—as expected for all superconductors—of approximately 40 parts per million at T_c . In contrast, the shear elastic moduli c_{44} , c_{55} and c_{66} show only changes in slope at T_c , consistent

with a single-component superconducting order parameter. Arrows mark the superconducting transition for all shear moduli. $\Delta c_{ii}/c_{ii}$ is defined as $(c_{ii}(T) - c_{ii}(T_0))/c_{ii}(T_0)$, where T_0 is the highest temperature shown.

Symmetry of the superconducting order parameter

The presence or absence of a discontinuity in each elastic modulus constrains the symmetry of the superconducting order parameter. Roughly speaking, only strains that couple linearly to a degree of freedom associated with the superconducting order parameter show discontinuities at $T_{\rm c}$. We illustrate this with a couple of examples; a more rigorous derivation is given in 'Landau free energy calculations' in Supplementary Information.

Discontinuities in elastic moduli arise when there is coupling between strain and superconductivity that is linear in strain and quadratic in the order parameter. For a single-component superconducting order parameter, this only occurs for compression strains²¹. A single-component order parameter can be written as $\eta = \eta_0 e^{i\phi}$, where η_0 is the magnitude of the gap (which may depend on momentum) and ϕ is the superconducting phase. The lowest-order coupling to a strain ϵ_{ij} is $\epsilon_{ij}\eta^*\eta = \epsilon_{ij}\eta_0^2$, where the asterisk denotes complex conjugation. This coupling is allowed only if ϵ_{ij} preserves the symmetry of the lattice; that is, it is only allowed for compression strains and not for shear

strains (which break the lattice symmetry). Since η_0^2 is proportional to the superfluid density, the physical interpretation of the resulting discontinuity at T_c is that compression strain couples to the superfluid density, which turns on at T_c and provides a new degree of freedom that softens the lattice.

In contrast to single-component order parameters, multi-component order parameters can have discontinuities in shear elastic moduli. This is because there are more degrees of freedom associated with a multi-component order parameter than with a single-component order parameter. Writing a two-component order parameter as $\vec{\eta} = \{\eta_{0,i}e^{i\phi_i},\eta_{0,j}e^{i\phi_j}\}$, there are now several possible couplings at lowest order. Taking the well-known $p_x + ip_y$ state in tetragonal crystals as an example, one possible coupling is $\epsilon_{xy}\eta_{0,p_x}\eta_{0,p_y}\cos\left(\phi_{p_x}-\phi_{p_y}\right)$. This is the so-called phase mode of the order parameter, as it couples ϵ_{xy} shear strain to the relative phase of the two components (Fig. 1). This produces a discontinuity in the associated elastic modulus c_{66} . The relative phase is a new degree of freedom that is only present in a multi-component order parameter, as strain

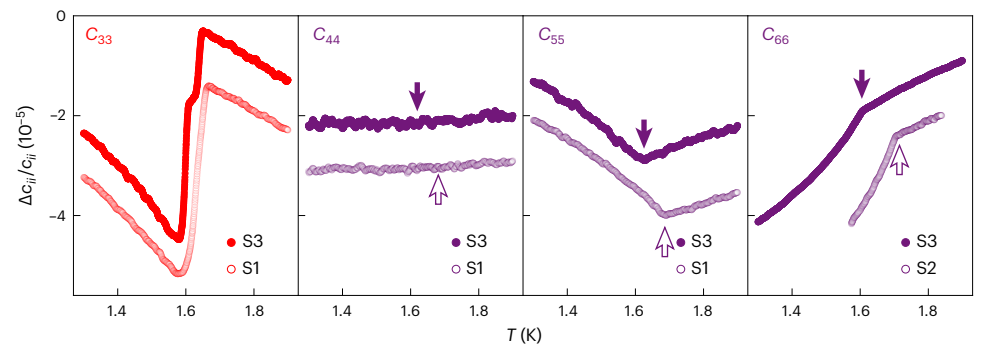


Fig. 3 | Relative change in elastic moduli through T_c for double- T_c UTe₂. The compressional elastic modulus c_{33} shows two distinct discontinuities at T_c , consistent with the two peaks we find in the specific heat of the same sample. The shear moduli, on the other hand, show no discontinuities and behave nearly identically to the shear moduli of the single- T_c sample. Single-(double-)transition

samples are shown with empty (filled) symbols. Empty (filled) arrows mark the superconducting transition for all shear moduli for single-(double-)transition samples. $\Delta c_{ii}/c_{ii}$ is defined as in Fig. 2, and curves have been offset vertically for clarity.

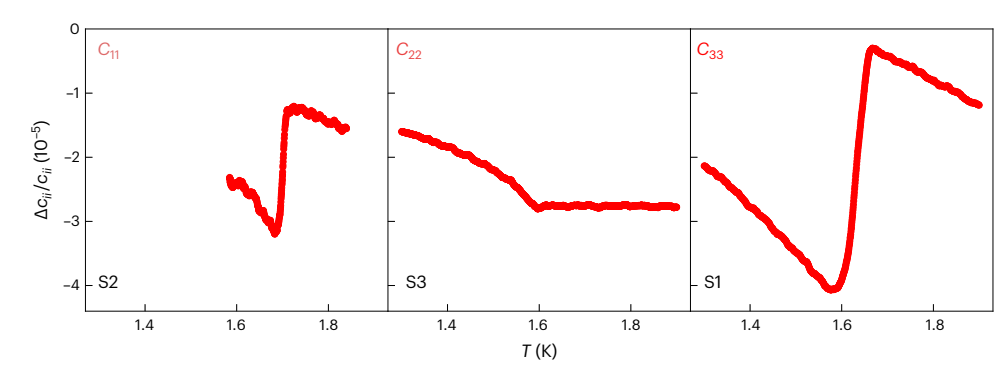


Fig. 4 | **Relative change in compressional elastic moduli through** T_c **.** The compressional elastic moduli as functions of temperature through T_c . c_{33} and c_{11} were measured on a single- T_c sample, and c_{22} was measured on the double- T_c sample. Both c_{11} and c_{33} show clearly resolvable discontinuities at T_c , whereas c_{22} shows a barely resolvable discontinuity. $\Delta c_{ij}/c_{ij}$ is defined as in Fig. 2.

cannot couple to the absolute phase of a single-component order parameter (such a term would break gauge symmetry). Similar expressions exist for orthorhombic crystals (see 'Landau free energy calculations' section in Supplementary Information for details), but the main conclusion is independent of the crystal structure: shear elastic moduli only exhibit discontinuities at $T_{\rm c}$ for multi-component superconducting order parameters.

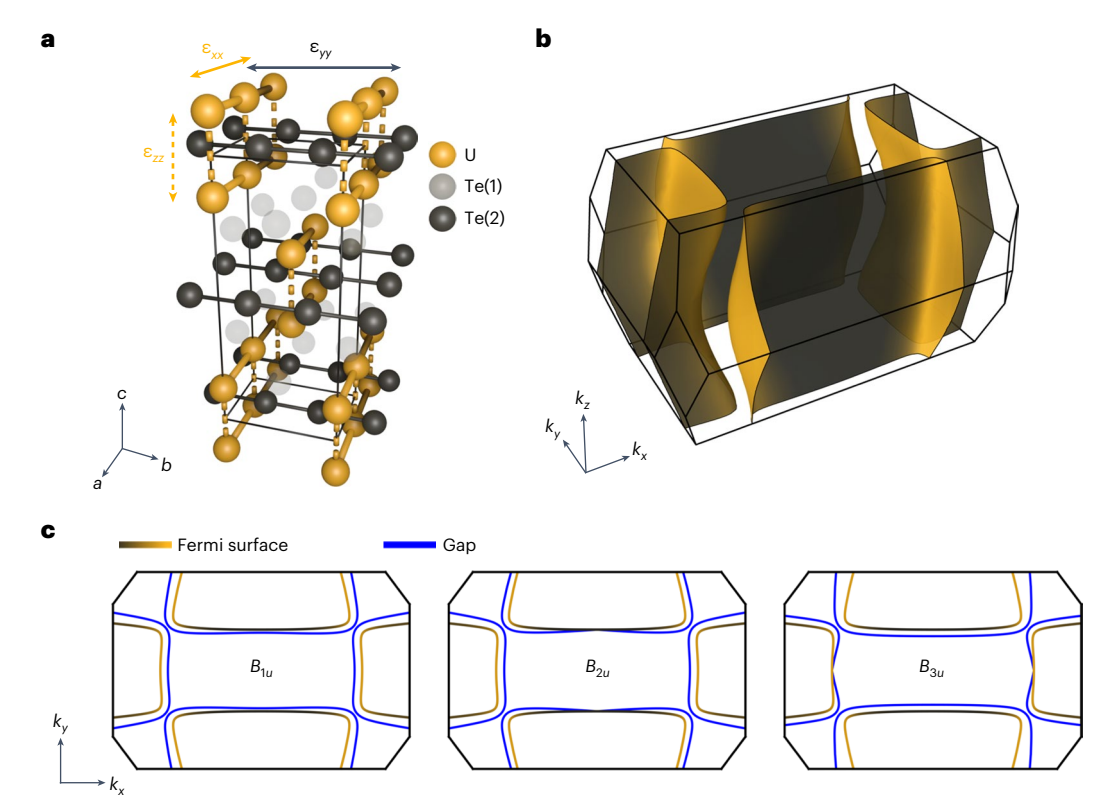
The absence of a discontinuity in any shear elastic modulus in the single-transition samples (S1 and S2) rules out essentially all two-component order parameters in UTe₂. While there are no natural two-component order parameters in UTe₂ because the crystal structure is orthorhombic, many nearly or accidentally degenerate order parameters have been proposed to explain the presence of the two nearly degenerate T_c 's, time reversal symmetry breaking and chiral surface states (Table 1). One proposal is the onset of first a B_{2u} state followed by a B_{3u} state at the second, lower T_c (refs. 12,13,22-24). This proposal predicts the usual discontinuities in compressional moduli at the first (higher) T_c , followed by a discontinuity in the compressional moduli and the $c_{\rm 66}$ shear modulus at the lower T_c . In fact, the product of any two odd-parity (that is *p*-or *f*-wave) states or any two even-parity (that is *s*-or *d*-wave) states in D_{2h} predicts a discontinuity in either c_{44} , c_{55} or c_{66} , none of which we observe. This strongly constrains the superconducting order parameter of UTe₂ to be of the single-component type. Finally, we note that our data are fully consistent with any single-component order parameter, including even-parity states such as s-wave and d-wave.

The similar absence of discontinuities in the shear elastic moduli of the two-transition sample (S3) rules out the multi-component explanation for the second superconducting transition. We find that the single discontinuity in c_{33} in single- T_c samples is approximately the same size as the sum of the two discontinuities found in double- T_c samples. This suggests that, below the second transition, all electrons in UTe, are in the same thermodynamic state, rather than double- T_c samples having two separate superconducting mechanisms. This suggests a common origin for the two superconducting transitions, perhaps split by local strains¹⁷ or magnetic impurities²⁵. Why this usually manifests as only two sharp T_c 's (as we also observe in our data), rather than as multiple T_c 's or as a broad transition, remains an open question. It also leaves unresolved the issue of why even single- T_c samples become double- T_c samples under hydrostatic pressure, leaving open the possibility of a multi-component order parameter under pressure.

Coupling of compression strains to superconductivity

The smallness of the discontinuity in c_{22} compared with the other two compressional moduli indicates that the superconductivity in UTe₂ is insensitive to strain along the b axis (c_{yy}). This observation is made quantitative through Ehrenfest relations, which relate discontinuities in the elastic moduli, δc_{ij} , to the discontinuity in the specific heat, ΔC . The Ehrenfest relations are

$$\delta c_{ij} = -\frac{\Delta C}{T} \left(\frac{\mathrm{d}T_{\mathrm{c}}}{\mathrm{d}\epsilon_{ij}} \right)^2,\tag{1}$$



 $\label{eq:Fig.5} \textbf{Influence of compression strains on the crystal structure and Fermi surface of UTe_2. a, The crystal structure of UTe_2. Highlighted are tellurium chains along the$ *b*axis and chains that run along the*a*axis consisting of*c*-axis-oriented uranium dimers. b, The geometry of the Fermi surface, modelled after quantum

oscillation measurements, which is dominated by the chains shown in \mathbf{a}^{27} . The Fermi surface is coloured according to its uranium (yellow) and tellurium (grey) content. \mathbf{c} , The superconducting gaps (blue lines) for three possible odd-parity order parameters at $k_z = 0$.

where $\frac{d\mathcal{T}_c}{d\varepsilon_{yj}}$ is the derivative taken at zero applied stress. Using the specific heat measured on sample S3 (Supplementary Figs. 7 and 8) and the data shown in Fig. 4, we calculate $\frac{d\mathcal{T}_c}{d\varepsilon_{xx}} = 0.23 \pm 0.02\,$ K per % strain, $\frac{d\mathcal{T}_c}{d\varepsilon_{yy}} = 0.07 \pm 0.02\,$ K per % strain and $\frac{d\mathcal{T}_c}{d\varepsilon_{zz}} = 0.34 \pm 0.02\,$ K per % strain.

These values are roughly consistent with those measured in uniaxial strain experiments²⁶ (see Supplementary Table 2 for a quantitative comparison).

These Ehrenfest relations indicate that the superconductivity of UTe₂ is substantially more sensitive to strains along the a and c axes than it is to strain along the b axis. This observation is perhaps surprising given the relatively quasi-two-dimensional nature of the Fermi surface measured by quantum oscillations in UTe₂ (refs. 27,28). This Fermi surface consists of two sets of quasi-one-dimensional sheets running along the a and b axes that hybridize to form one electron and one hole pocket (Fig. 5). Thus, if any direction is to be weakly coupled to superconductivity, one might expect it to be the c axis. This argument is unchanged by the possible existence of an additional small pocket of Fermi surface reported by Broyles et al. 29 , as it is roughly isotropic and thus does not single out any particular direction.

Looking at the crystal structure in Fig. 5, however, it is clear that the a and b axes are very different: chains of c-axis-coupled uranium dimers run along the a axis, whereas chains of tellurium run along the b axis (the other tellurium site, Te(1), participates much less in the Fermi surface than the Te(2) chains; Supplementary Figs. 9 and 10). Thus, ϵ_{xx} and ϵ_{zz} modulate the inter- and intra-dimer coupling of the uranium dimers, respectively, whereas ϵ_{yy} only modulates the weak inter-chain coupling of the uranium chains. ϵ_{yy} does, however, modulate the spacing between tellurium atoms in the tellurium chains that run along the b axis. Our observation of the relative insensitivity of T_c to ϵ_{yy} therefore

suggests that the superconducting pairing is more sensitive to the uranium–uranium distances than to the tellurium–tellurium distances.

Proposed single-component superconducting order parameter

Thermal transport⁶, specific heat^{7,9} and penetration depth⁸ all suggest the presence of point nodes in the superconducting gap of UTe₂. B_{1u} , B_{2u} and B_{3u} order parameters all have point nodes in their superconducting gaps, but these nodes lie along different directions in momentum space and thus intersect different portions of the Fermi surface (or may not intersect the Fermi surface at all if it is quasi-2D).

We use our observation of relatively weak coupling between ϵ_{yy} and T_c to motivate a particular orientation of the point nodes in UTe₂ and to suggest one particular single-component order parameter. Figure 5 shows a tight binding model of the Fermi surface of UTe₂ as determined by quantum oscillations, colour-coded by the relative uranium 6d and tellurium 5p content (both bands have substantial uranium 5f character that contributes to their heavy masses but not to their geometry). Our results suggest that the superconducting gap is either weak or absent on the tellurium-dominant electron Fermi surface. Only the B_{2u} order parameter has nodes that lie along the k_y direction, producing a node in the gap on the tellurium-dominant surface and a gap maximum on the uranium-dominant surface. We note that a reported small pocket with a light mass does not qualitatively affect this argument $ext{2}$, as it is largely isotropic in shape and thus will not respond differently to $ext{2}$ and $ext{2}$ systrain.

Discussion

Our discovery of a single-component order parameter places strong constraints on possible explanations for other experimental observations. First, a single-component order parameter cannot break

time reversal symmetry. This suggests that the interpretation of time reversal symmetry breaking at $T_{\rm c}$ as seen by polar Kerr effect measurements ^{12,13}, along with the chiral surface states seen in STM ¹⁴ and microwave surface impedance measurements ¹⁵, needs to be revisited.

The search for multi-component superconductors continues: they are of both fundamental and practical interest, since a multi-component order parameter is a straightforward route to topological superconductivity. We find that, while UTe₂ may have an odd-parity, spin-triplet order parameter, it seems that the most likely order parameter to condense at T_c is of the single-component B_{2u} representation: either p_y - or f_{yz^2} -wave superconductivity. Definitive determination of the orientation of the nodes in the superconducting gap would confirm this scenario.

Online content

Any methods, additional references, Nature Portfolio reporting summaries, source data, extended data, supplementary information, acknowledgements, peer review information; details of author contributions and competing interests; and statements of data and code availability are available at https://doi.org/10.1038/s41567-024-02493-1.

References

- Tsuei, C. C. & Kirtley, J. R. Pairing symmetry in cuprate superconductors. Rev. Mod. Phys. 72, 969–1016 (2000).
- Ghosh, S. et al. Thermodynamic evidence for a two-component superconducting order parameter in Sr₂RuO₄. Nat. Phys. 17, 199–204 (2021).
- 3. Rice, T. M. & Sigrist, M. Sr_2RuO_4 : an electronic analogue of 3He ? J. Phys. Condensed Matter **7**, L643–L648 (1995).
- Mackenzie, A. P., Scaffidi, T., Hicks, C. W. & Maeno, Y. Even odder after twenty-three years: the superconducting order parameter puzzle of Sr₂RuO₄. npj Quantum Mater. 2, 40 (2017).
- Sato, M. & Ando, Y. Topological superconductors: a review. Rep. Prog. Phys. 80, 076501 (2017).
- Metz, T. et al. Point-node gap structure of the spin-triplet superconductor UTe₂. Phys. Rev. B 100, 220504 (2019).
- Ran, S. et al. Nearly ferromagnetic spin-triplet superconductivity. Science 365, 684–687 (2019).
- Ishihara, K. et al. Chiral superconductivity in UTe₂ probed by anisotropic low-energy excitations. Nat. Commun. 14, 2966 (2023).
- Kittaka, S. et al. Orientation of point nodes and nonunitary triplet pairing tuned by the easy-axis magnetization in UTe₂. Phys. Rev. Res. 2, 032014 (2020).
- Aoki, D. et al. Unconventional superconductivity in heavy fermion UTe₂. J. Phys. Soc. Jpn 88, 043702 (2019).
- 11. Ran, S. et al. Extreme magnetic field-boosted superconductivity. *Nat. Phys.* **15**, 1250–1254 (2019).
- Hayes, I. M. et al. Multicomponent superconducting order parameter in UTe₂. Science 373, 797–801 (2021).
- Wei, D. S. et al. Interplay between magnetism and superconductivity in UTe₂. Phys. Rev. B 105, 024521 (2022).
- Jiao, L. et al. Chiral superconductivity in heavy-fermion metal UTe₂. Nature 579, 523–527 (2020).
- Bae, S. et al. Anomalous normal fluid response in a chiral superconductor UTe₂. Nat. Commun. 12, 2644 (2021).
- Rosa, PriscilaF. S. et al. Single thermodynamic transition at 2K in superconducting UTe₂ single crystals. Commun. Mater. 3, 1–6 (2022).
- Thomas, S. M. et al. Spatially inhomogeneous superconductivity in UTe₂. Phys. Rev. B 104, 224501 (2021).
- Aoki, D. et al. Multiple superconducting phases and unusual enhancement of the upper critical field in UTe₂. J. Phys. Soc. Jpn 89, 053705 (2020).

- Braithwaite, D. et al. Multiple superconducting phases in a nearly ferromagnetic system. Commun. Phys. 2, 147 (2019).
- Ushida, K. et al. Lattice instability of UTe₂ studied by ultrasonic measurements. JPS Conf. Proc. 38, 011021 (2023).
- Rehwald, W. The study of structural phase transitions by means of ultrasonic experiments. Adv. Phys. 22, 721–755 (1973).
- Shishidou, T., Suh, HanGyeol, Brydon, P. M. R., Weinert, M. & Agterberg, D. F. Topological band and superconductivity in UTe₂. Phys. Rev. B 103, 104504 (2021).
- 23. Choi, H. C., Lee, S. H., & Yang, B.-J. Correlated normal state fermiology and topological superconductivity in UTe₂. Preprint at https://arxiv.org/abs/2206.04876 (2023).
- 24. Shaffer, D. & Chichinadze, D. V. Chiral superconductivity in UTe_2 via emergent C_4 symmetry and spin-orbit coupling. *Phys. Rev. B* **106**, 014502 (2022).
- Sundar, S. et al. Ubiquitous spin freezing in the superconducting state of UTe₂. Commun. Phys. 6, 24–34 (2023).
- Girod, Clément et al. Thermodynamic and electrical transport properties of UTe₂ under uniaxial stress. *Phys. Rev. B* 106, L121101 (2022).
- 27. Eaton, A. G. et al. Quasi-2D Fermi surface in the anomalous superconductor UTe₂. *Nat. Commun.* **15**, 223 (2024).
- Aoki, D. et al. First observation of the de Haas-van Alphen effect and Fermi surfaces in the unconventional superconductor UTe₂. J. Phys. Soc. Jpn 91, 083704 (2022).
- Broyles, C. et al. Revealing a 3D Fermi surface pocket and electron-hole tunneling in UTe₂ with quantum oscillations. Phys. Rev. Lett. 131, 036501 (2023).
- 30. Matsumura, H. et al. Large reduction in the *a*-axis Knight shift on UTe₂ with T_c =2.1K. *J. Phys. Soc. Jpn* **92**, 063701 (2023).
- Iguchi, Y. et al. Microscopic imaging homogeneous and single phase superfluid density in UTe₂. Phys. Rev. Lett. 130, 196003 (2023).
- Xu, Y., Sheng, Y. & Yang, Yi-feng Quasi-two-dimensional Fermi surfaces and unitary spin-triplet pairing in the heavy fermion superconductor UTe₂. Phys. Rev. Lett. 123, 217002 (2019).
- Fujibayashi, H. et al. Superconducting order parameter in UTe₂ determined by Knight shift measurement. J. Phys. Soc. Jpn 91, 043705 (2022).
- Nakamine, G. et al. Anisotropic response of spin susceptibility in the superconducting state of UTe₂ probed with ¹²⁵Te-NMR measurement. *Phys. Rev. B* 103, L100503 (2021).
- Nakamine, G. et al. Inhomogeneous superconducting state probed by ¹²⁵Te NMR on UTe₂. J. Phys. Soc. Jpn 90, 064709 (2021).
- 36. Machida, K. Theory of spin-polarized superconductors—an analogue of superfluid ³He A-phase. *J. Phys. Soc. Jpn* **89**, 033702 (2020).
- Machida, K. Nonunitary triplet superconductivity tuned by field-controlled magnetization: URhGe, UCoGe, and UTe₂. Phys. Rev. B 104, 014514 (2021).
- 38. Nevidomskyy, A. H. Stability of a nonunitary triplet pairing on the border of magnetism in UTe₂. Preprint at https://arxiv.org/abs/2001.02699 (2020).
- Ishizuka, J., Sumita, S., Daido, A. & Yanase, Y. Insulator-metal transition and topological superconductivity in UTe₂ from a first-principles calculation. *Phys. Rev. Lett.* 123, 217001 (2019).
- Hazra, T. & Volkov, P. Pair-Kondo effect: a mechanism for time-reversal broken superconductivity and finite-momentum pairing in UTe₂. Preprint at https://arxiv.org/abs/2210.16293 (2022).
- 41. Chang, Y.-Y. et al. Topological Kondo superconductors. Preprint at https://arxiv.org/abs/2301.00538 (2023).

Publisher's note Springer Nature remains neutral with regard to jurisdictional claims in published maps and institutional affiliations.

Springer Nature or its licensor (e.g. a society or other partner) holds exclusive rights to this article under a publishing agreement with

the author(s) or other rightsholder(s); author self-archiving of the accepted manuscript version of this article is solely governed by the terms of such publishing agreement and applicable law.

@ The Author(s), under exclusive licence to Springer Nature Limited 2024

Methods

Sample growth and preparation

Single crystals of UTe₂ were grown by the chemical vapour transport method as described in refs. 7,42. Samples with one T_c (two T_c 's) were grown in a two-zone tube furnace with temperatures of 950 °C and 860 °C (1,060 °C and 1,000 °C) at the hot and cold end, respectively.

Specimens were aligned to better than 1° using their magnetic anisotropy (performed in a Quantum Design MPMS) and X-ray diffraction (performed in a Laue backscattering system) measurements. Samples were then polished to produce two parallel faces normal to the (100), (010) and (001) directions, depending on the mode geometry (Extended Data Table 1).

Thin-film ZnO piezoelectric transducers were sputtered from a ZnO target in an atmosphere of oxygen and argon. Both shear and longitudinal responses are present in each transducer—the shear axis was aligned with either (100), (010) or (001), again depending on the particular mode geometry. Three crystals were measured in total (see Extended Data Table 1 for details). The shear response in our deposited transducers was achieved by mounting the sample on the far end of the sputtering sample stage, maximizing the distance between the sample and the ZnO target. The position of the sample stage was fixed during the entire deposition process (that is, rotation was disabled on the sample stage). The resulting polarization direction of the generated sound wave is then parallel to the shortest line drawn between the sample and the target—this orientation was verified using the absolute speed of sound and the moduli obtained using resonant ultrasound spectroscopy⁴³.

Pulse-echo ultrasound measurements

Measurements were performed in an Oxford Instruments Heliox 3 He refrigerator. We used a traditional phase-comparison pulse-echo ultrasound method to measure the change in elastic moduli relative to the highest temperature T_0 ; that is, we measured $\Delta c/c \equiv (c(T) - c(T_0))/c(T_0)$ Short bursts (typically -50 ns) of radiofrequency signals, with the carrier frequency between 500 MHz and 2.5 GHz, were generated with a Tektronix TSG 4106A RF generator modulated by a Tektronix AFG 31052 arbitrary function generator, amplified by a Mini-Circuits ZHL-42W+ power amplifier, and transmitted to the transducer. The signal was detected with the same transducer, amplified with a Mini-Circuits ZX60-3018G-S+ amplifier and recorded on a Tektronix MSO64 oscilloscope. The detection amplifier was isolated from the power amplifier using Mini-Circuits ZFSWA2-63DR+ switches, timed with the same Tektronix AFG 31052 arbitrary function generator.

Both shear and compressional sound are generated by our transducers—these signals are separated in the time domain owing to the different speeds of propagation and identified as shear or compression using the known elastic moduli of UTe₂ (ref. 43). Extended Data Fig. 1 shows a raw pulse-echo signal from a transducer sputtered on sample S3 with sound propagating along the [010] direction with a shear polarization axis along [100], thus measuring c_{22} and c_{66} simultaneously. Echoes corresponding to the different elastic modes can be clearly identified as shear (vertical dashed red lines) and compression (vertical dashed blue lines).

The phase of each echo was analysed using a software lock-in, and the relative change in phase between two echoes was converted to the relative change in speed of sound as a function of temperature. In Extended Data Fig. 2, we compare the temperature dependence of c_{33} of samples S1 and S3 obtained with different transducers.

Data availability

Data that support the plots within this paper and other findings of this study are available via GitHub at https://github.com/CHiLL-Ramshaw/manuscripts-supporting_data/tree/0292ab9b15b6 0af93341e64b759507e4e59eb7cd/2024_Single_Component_Superconductivity_in_UTe2_at_Ambient_Pressure (ref. 44) and from the

corresponding author upon reasonable request. Source data are provided with this paper.

References

- 42. Ran, S. et al. Comparison of two different synthesis methods of single crystals of superconducting uranium ditelluride. *J. Vis. Exp.* https://doi.org/10.3791/62563 (2021).
- 43. Theuss, F. et al. Resonant ultrasound spectroscopy for irregularly shaped samples and its application to uranium ditelluride. *Phys. Rev. Lett.* **132**, 066003 (2024).
- 44. Theuss, et al. 2024_single_component_superconductivity_ in_UTe₂_at_ambient_pressure. GitHub https://github.com/ CHiLL-Ramshaw/manuscripts-supporting_data/tree/0292ab9b15 b60af93341e64b759507e4e59eb7cd/2024_Single_Component_ Superconductivity in UTe2 at Ambient Pressure (2024).

Acknowledgements

We acknowledge helpful discussions with D. Agterberg and P. Brydon. We thank the Cornell LASSP Professional Machine Shop for their contributions to designing and fabricating equipment used in this study. A. Shragai, B.J.R. and F.T. acknowledge funding from the Office of Basic Energy Sciences of the United States Department of Energy under award number DE-SC0020143 (ultrasound experiments and analysis). N.P.B. and J.P. acknowledge support from the Department of Energy award number DE-SC-0019154 (sample characterization), the Gordon and Betty Moore Foundation's EPiQS Initiative through grant number GBMF9071 (materials synthesis), the National Science Foundation under grant number DMR-2105191 (sample preparation) and the Maryland Quantum Materials Center and the National Institute of Standards and Technology. B.J.R. and F.T. acknowledge use of the Cornell Center for Materials Research Shared Facilities which are supported through the NSF MRSEC programme (DMR-1719875). G.G. acknowledges support from the ANR grants STeP2 no ANR-22-EXES-0013 and QuantEx no ANR-23-CE30-0001-01.

Author contributions

B.J.R. conceived the experiment. I.M.H., S.R.S., Y.S.E. and A. Suarez grew and characterized the samples. F.T. and A. Shragai performed the sample preparation and transducer fabrication. F.T., A. Shragai and G.G. performed the ultrasound measurements. F.T. and B.J.R. performed the data analysis and mean-field calculations. T.S. performed density functional theory calculations. F.T. and B.J.R. wrote the paper with input from all other co-authors. J.P., N.P.B. and B.J.R. supervised the project.

Competing interests

The authors declare no competing interests.

Additional information

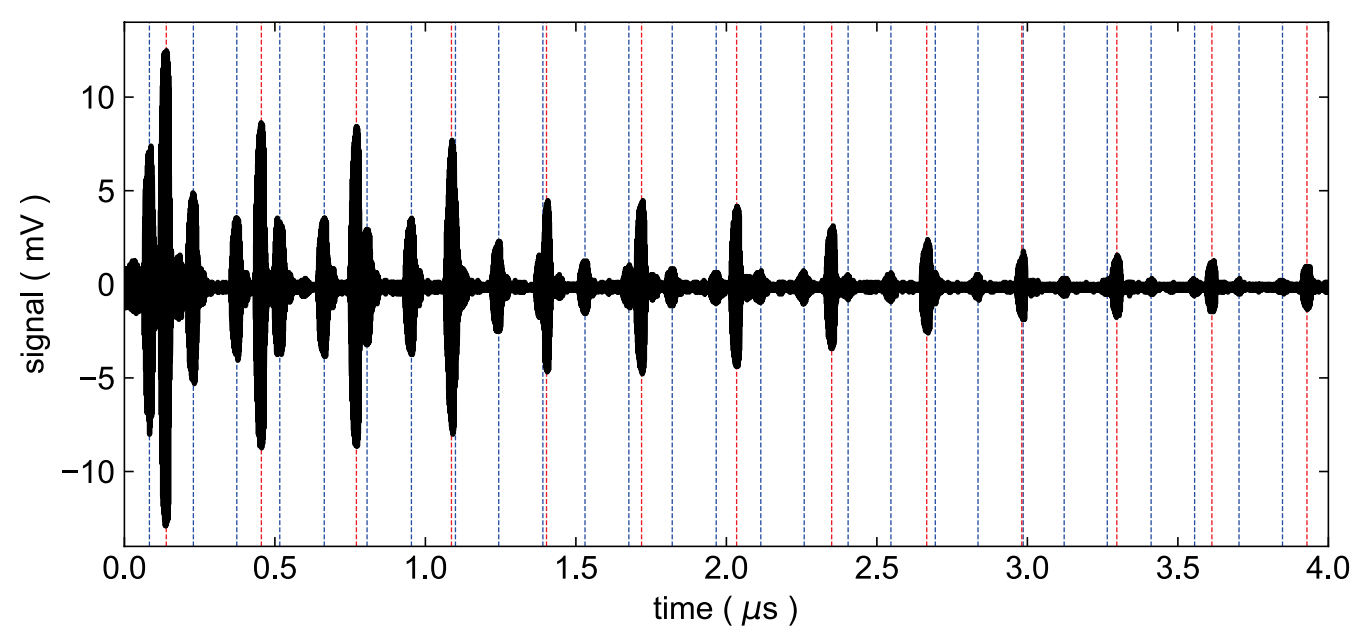
Extended data is available for this paper at https://doi.org/10.1038/s41567-024-02493-1.

Supplementary information The online version contains supplementary material available at https://doi.org/10.1038/s41567-024-02493-1.

Correspondence and requests for materials should be addressed to B. J. Ramshaw.

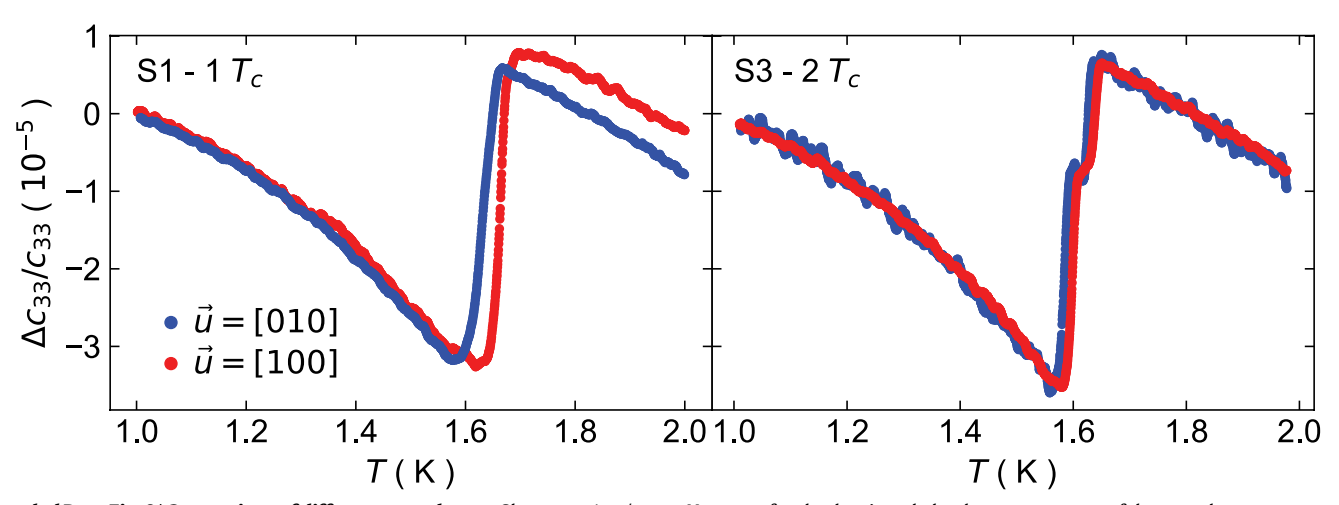
Peer review information *Nature Physics* thanks Tatsuya Yanagisawa and the other, anonymous, reviewer(s) for their contribution to the peer review of this work.

Reprints and permissions information is available at www.nature.com/reprints.



 $\label{lem:condition} \textbf{Extended Data Fig. 1} | \textbf{Raw Pulse-Echo Signal.} \text{ The raw signal from a sputtered} \\ \textbf{ZnO shear transducer on sample S3 with sound propagation along the [010]} \\ \textbf{and polarization along the [100] directions.} \text{ The transducer exhibits both a} \\ \textbf{And the polarization along the [100] directions.} \\ \textbf{And the polarization along the [100] di$

compressional (blue lines) and a shear (red dashed lines) response. These correspond to sound modes determined by the elastic moduli c_{22} and c_{66} , respectively.



Extended Data Fig. 2 | **Comparison of different transducers.** Shown are $\Delta c_{33}/c_{33}$ for single T_c (S1, left) and two T_c (S3, right) samples. For each sample we compare the relative change in elastic modulus between measurements obtained with two different transducers. Both transducers excited sound along the [001] direction.

However, for the data in red, the shear component of the transducer was polarized along [100] (additionally measuring $c_{\rm 55}$), whereas for the data in blue, the shear component of the transducer was polarized along [010] (additionally measuring $c_{\rm 44}$).

Extended Data Table 1 | Pulse-echo ultrasound sample configurations

$\# T_c$	Sample	$ec{k}$	\vec{u}	c_{ij}	f (MHz)	$d~(\mu \mathrm{m})$	c (GPa)
1	S1	[001]	[100] [010] [001]	$c_{55} \\ c_{44} \\ c_{33}$	1261 1434 2260	330 ± 17 330 ± 17 330 ± 17	51 ± 5 27 ± 3 91 ± 11
	S2	[100]	[100] [010]	$c_{11} \\ c_{66}$	823 1250	920 ± 46 920 ± 46	81 ± 8 28 ± 3
2	S3	[001]	[100] [010] [001]	c_{55} c_{44} c_{33}	1348 1352 1348	550 ± 28 550 ± 28 550 ± 28	52 ± 5 28 ± 3 88 ± 9
		[010]	[100] [010]	$c_{66} \\ c_{22}$	$1362 \\ 1362$	290 ± 15 290 ± 15	30 ± 3 141 ± 15

Listed are the transducer configurations for all the measurements in this manuscript. Samples are sorted by the number of superconducting phase transitions (first column). Additional information given is the propagation \vec{k} and the polarization \vec{u} of the sound pulse excited in the sample, as well as the measured elastic modulus. Also shown is the frequency at which each measurement is performed. We also provide the thicknesses d of the measured samples and the resulting absolute values of the elastic moduli obtained from the separation of echoes at room temperature. Uncertainties represent a 5% uncertainty in the thickness.